

Onset of treelike patterns in negative streamers

M. Arrayás,¹ M. A. Fontelos,² and U. Kindelán³¹Área de Electromagnetismo, Universidad Rey Juan Carlos, Camino del Molino s/n, 28943 Fuenlabrada, Madrid, Spain²Instituto de Ciencias Matemáticas (CSIC-UAM-UCM-UC3M), C/Nicolás Cabrera, 28049 Madrid, Spain³Departamento de Matemática Aplicada y Met. Inf., Universidad Politécnica de Madrid, Alenza 4, 28003 Madrid, Spain

(Received 7 February 2012; revised manuscript received 27 September 2012; published 14 December 2012)

We present analytical and numerical studies of the initial stage of the branching process based on an interface dynamics streamer model in the fully three-dimensional case. This model follows from fundamental considerations on charge production by impact ionization and balance laws, and leads to an equation for the evolution of the interface between ionized and nonionized regions. We compare some experimental patterns with the numerically simulated ones, and give an explicit expression for the growth rate of harmonic modes associated with the perturbation of a symmetrically expanding discharge. By means of full numerical simulation, the splitting and formation of characteristic treelike patterns of electric discharges is observed and described.

DOI: [10.1103/PhysRevE.86.066407](https://doi.org/10.1103/PhysRevE.86.066407)

PACS number(s): 52.80.Hc, 47.54.-r, 51.50.+v

I. INTRODUCTION

It is a well known visible fact that electric discharges form treelike patterns, very much like those in coral reefs and snowflakes. The study of the branching process leading to such patterns is of considerable interest both from pure and applied points of view. Many industrial techniques, ranging from lasers to chemical processing of gases and water purification could be improved provided the development of treelike patterns can be controlled or avoided. Although an electric discharge is a very complex phenomenon, with radiation and chemistry processes involved [1–3], the description of its initial stage is simpler. A single free electron traveling in a strong, uniform electric field ionizes the gaseous molecules around it, generating more electrons and starting a chain reaction of ionization. The ionized gas creates its own electric field, which speeds up the reaction, and a streamer is born. The streamers of ionized gas have an inevitable tendency to break up at their tips, followed by the creation of the familiar treelike pattern.

Early efforts [4–7] were able to identify a minimal streamer model with which, after numerical simulations under the hypothesis of cylindrical symmetry, an instability was observed [8–10]. Later on, the dispersion relation for planar fronts was computed and the existence of an instability leading to the development of fingers was found [11]. Due to the enormous difficulty in performing full numerical simulations of the streamers model, some different approaches have been attempted in recent years (see [12,13] for a review where various different approaches are discussed and a very thorough mathematical analysis of the contour problem by the moving boundary expert Saleh Tanveer with coauthors is referred to; see also [14,15]). The influence of microscopic corrections such as photoionization or local electron density fluctuations has been addressed and incorporated into the models and corresponding simulations, showing acceleration of the ionization front (cf. [16–19]).

In any case, the fully three-dimensional (3D) case has proved to be very difficult. As an alternative approach (the one we follow in this work), the motion and propagation of the streamer discharge has recently been described by a contour dynamics model first introduced in Ref. [20] and used to successfully predict some experimental features of discharges

on dielectric surfaces [21,22]. The contour dynamics model describes the interface separating a plasma region from a neutral gas region. For a negative discharge, the separating surface has a net charge σ and the thickness goes to zero as \sqrt{D} , with D the charge diffusion coefficient. The interface moves with a velocity in the normal direction

$$v_N = -\mu_e E_v^+ + 2\sqrt{\frac{D_e}{l_0} \mu_e |E_v^+| \exp\left(-\frac{E_{\text{ion}}}{|E_v^+|}\right)} - D_e \kappa, \quad (1)$$

where E_v^+ is the normal component of the electric field at the interface when approaching it from outside the plasma region, μ_e is the electron mobility, D_e is the electron diffusion coefficient, E_{ion} is a characteristic ionization electric field, and κ is twice the mean curvature of the interface. The parameter l_0 is the microscopic ionization characteristic length.

The total negative surface charge density at the interface changes according to

$$\frac{\partial \sigma_e}{\partial t} + \kappa v_N \sigma_e = -\frac{E_v^-}{\varrho_e} - j_v^-, \quad (2)$$

where E_v^- is the electric field at the interface coming from inside the plasma, ϱ_e is a parameter proportional to the resistivity of the electrons in the created plasma, and j_v^- is the current contribution at the surface of any source inside the plasma. For instance, an insulated wire inside the plasma at \mathbf{x}_0 , carrying an electric current $I(t)$, will create a current density inside the plasma and as quasineutrality is fulfilled, for the plasma region we will have

$$\nabla \cdot \mathbf{j} = I(t)\delta(\mathbf{x} - \mathbf{x}_0), \quad (3)$$

and \mathbf{j} is obtained solving that equation. Note that at the interface there is an electric field discontinuity given by

$$E_v^+ - E_v^- = -\frac{e\sigma}{\epsilon_0}. \quad (4)$$

Using the contour dynamics model, we first present the simulations and the onset of the treelike patterns. Then we proceed by studying the stability of the interface and show how the instability grows calculating the dispersion curve, which gives information about the stability-instability of transversal modes. We end with some discussions about the experimental

predictions in two-dimensional (2D) and 3D situations and some remarks.

The technical details are left for the Appendix. There, the spherical discharge in the case of finite conductivity, the stability analysis, and the analytical limits of infinite resistivity and ideal conductivity are presented in some detail. The numerical method is also described in more detail.

II. SIMULATIONS AND THE SPLITTING OF FINGERS

In this section we present the numerical studies of the initial stage of the branching process based on an interface dynamics streamer model in the fully 3D case. The splitting and formation of characteristic treelike patterns of electric discharges is observed and described.

It is convenient to express the model in dimensionless units. The physical scales are given by the ionization length l_0 , the characteristic impact ionization field E_i , and the electron mobility μ_e . The velocity scale yields $U_0 = \mu_e E_i$, and the time scale $\tau_0 = l_0/U_0$. Typical values of these quantities for nitrogen at normal conditions are $l_0 \approx 2.3 \mu\text{m}$, $E_i \approx 200 \text{ kV/m}$, and $\mu_e \approx 380 \text{ cm}^2/\text{V s}$. The unit for the negative surface density reads $\sigma_0 = \epsilon_0 E_i/e$; so for the current density $j_0 = \sigma_0 U_0/l_0$ and for the resistivity $\varrho_0 = \mu_e l_0/\sigma_0$. The diffusion constant unit becomes $D_0 = l_0 U_0$. Introducing dimensionless units, the model reads

$$v_N = -E_v^+ + 2\sqrt{\varepsilon\alpha(|E_v^+|)} - \varepsilon\kappa, \quad (5)$$

$$\frac{\partial\sigma}{\partial t} + \kappa v_N \sigma = -\frac{E_v^-}{\varrho} - j_v^-, \quad (6)$$

being that

$$\alpha(|E_v^+|) = |E_v^+| \exp\left(-\frac{1}{|E_v^+|}\right), \quad (7)$$

and $\varepsilon = D_e/D_0$ the dimensionless diffusion coefficient. In what follows all the quantities are dimensionless unless otherwise indicated. We have used an adaptive boundary element method, developed for general contour dynamics problems [23,24], in order to perform numerical simulations with Eqs. (5) and (6). Here we present numerical results assuming that the plasma is ideally conducting, so that E_v^+ is computed by solving the Laplace equation with the following boundary conditions: (1) V behaves linearly at infinity, where a constant electric field is imposed and (2) $V = V_0$ constant at the plasma surface (with the constant to be determined from the condition that the net charge is given). The key point of the numerical simulation is the calculation of the charge density, proportional to E_v^+ in the case of an ideal conductor: We can write the potential V as

$$V = -Ex_3 + V',$$

where

$$\Delta V' = 0 \quad \text{outside } \Omega(t), \quad (8)$$

$$V' = Ex_3 + V_0 \quad \text{at the boundary of } \Omega(t), \quad (9)$$

$$V' = O(|\mathbf{x}|^{-1}) \quad \text{as } |\mathbf{x}| \rightarrow \infty, \quad (10)$$

E is the electric field fixed at infinity, and $\Omega(t)$ is the domain occupied by the plasma. The equation for the charge density

at the points $\mathbf{x}_0 = (x_{0,1}, x_{0,2}, x_{0,3})$ of the plasma interface is

$$V(\mathbf{x}_0) = \frac{1}{4\pi\epsilon_0} \int_{\partial\Omega(t)} \frac{\sigma(\mathbf{x})}{|\mathbf{x} - \mathbf{x}_0|} dS(\mathbf{x}) - Ex_{0,3} \quad (11)$$

or, since $V(\mathbf{x}_0)$ is constant,

$$Ex_{0,3} + V_0 = \frac{1}{4\pi\epsilon_0} \int_{\partial\Omega(t)} \frac{\sigma(\mathbf{x})}{|\mathbf{x} - \mathbf{x}_0|} dS(\mathbf{x}) \quad (12)$$

and we can write $\sigma = V_0\sigma_0 + \sigma_{\text{ind}}$, where σ_{ind} is the charge density induced by the external electric field and defined as the solution to the integral equation

$$Ex_{0,3} = \frac{1}{4\pi\epsilon_0} \int_{\partial\Omega(t)} \frac{\sigma_{\text{ind}}(\mathbf{x})}{|\mathbf{x} - \mathbf{x}_0|} dS(\mathbf{x}) \quad (13)$$

and σ_0 is therefore the solution to

$$1 = \frac{1}{4\pi\epsilon_0} \int_{\partial\Omega(t)} \frac{\sigma_0(\mathbf{x})}{|\mathbf{x} - \mathbf{x}_0|} dS(\mathbf{x}). \quad (14)$$

The constant V_0 is determined by the condition

$$Q = V_0 \int_{\partial\Omega(t)} \sigma_0(\mathbf{x}) dS(\mathbf{x}) + \int_{\partial\Omega(t)} \sigma_{\text{ind}}(\mathbf{x}) dS(\mathbf{x}), \quad (15)$$

where Q is kept constant during the simulation.

In Fig. 1 we show numerical simulations of the evolution of the discharge at four time steps. The plasma is charged with integrated surface charge $Q = -25$, subject to an external field in the vertical direction $E = 0.5$, and confined inside an initially spherical geometry perturbed by $r_0(\theta, \phi) = R_0 + \delta_0 \exp\{-[\cos^2(\phi) + \cos^2(\theta)]/c\}$, with $R_0 = 1$, $c = 0.03$, and $\delta_0 = 0.1$. We first observe the onset of streamer fingers. At time $t = 0.17$ the streamers develop further instabilities and split again. Qualitatively the process can be described in the following terms: Any protuberance that develops is accompanied by an increase of the charge density at its tip. The electrostatic repulsion of charges at the tip tends to make the tip expand and the finger grow. In opposition to this is the action of the surface tension tending to flatten the protuberance and setting up a flux of charge from the protuberance out to the sides. However, overall, the protuberance becomes amplified. This process occurs again and again until a treelike pattern is produced. In Fig. 2 we depict a detail of this pattern (see also [25] for the development of this multiple branching process). Those ideas were anticipated in Ref. [8], but due to the restriction of 2D simulations the whole process of the branching pattern formation could not be observed.

III. INSTABILITY GROWTH AND THE DISPERSION CURVE

In this section we will make a linear perturbation analysis in order to show that the results of the numerical simulations can be anticipated and some features predicted. In order to be quantitative, we can calculate the growth rate of the different modes, both analytically and numerically. If an initial spherical symmetry interface is perturbed by a small amount, some instabilities will start growing. We will study which instability modes are going to prevail during the front evolution.

We consider a spherically expanding plasma, representing a corona discharge, with $Q(t) < 0$ so that $E_0 = E_v^+ = \frac{Q(t)}{4\pi R(t)^2} < 0$.

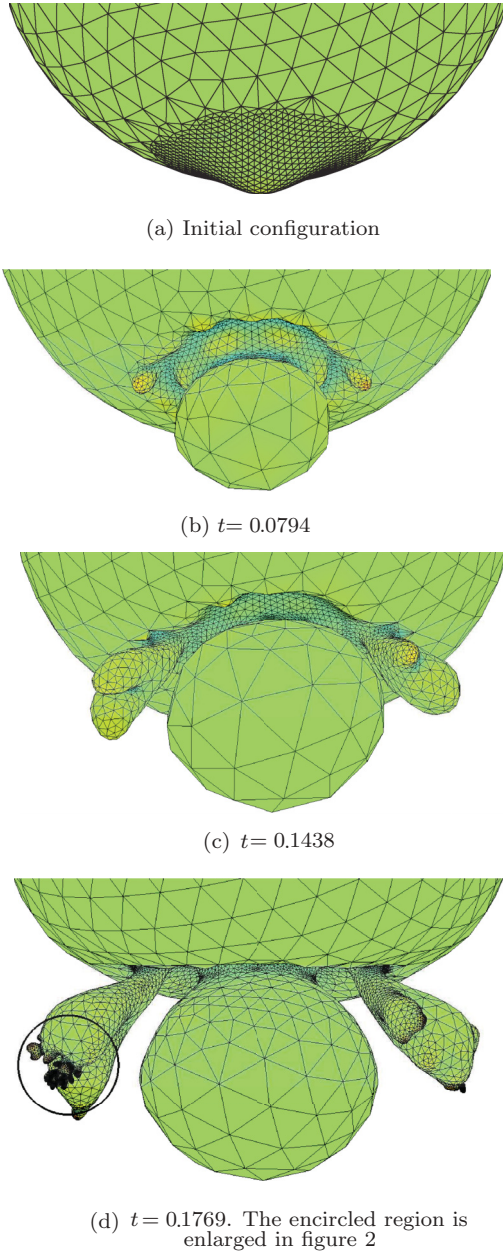


FIG. 1. (Color online) Evolution of the plasma for $Q = -25$, $E = 0.5$, and $\varepsilon = 0.02$. Color gradation represents curvature. The initial perturbation is a bump concentrated in $\theta = \pi$ for $\phi \in [0, 2\pi]$.

Then, $R(t)$ is given as the solution of

$$\frac{dR}{dt} = -\left(\frac{Q(t)}{4\pi R} + 2\varepsilon\right) \frac{1}{R} + 2\varepsilon^{1/2} \sqrt{\alpha(|E_v^+|)}. \quad (16)$$

$$\begin{aligned} \frac{db_{lm}}{dt} = & \frac{(l^2 - 1)E_0}{(2l + 1)R} \left[2E_0 + \frac{(l + 4)\varepsilon}{R} - (\varepsilon\alpha_0)^{1/2} \left(3 + \frac{1}{|E_0|} \right) \right] s_{lm} - \frac{I(t)(l + 1)}{4\pi R^2(2l + 1)} s_{lm} \\ & + \left[\frac{(l^2 + 4l + 2)}{(2l + 1)} E_0 + \frac{2\varepsilon}{R} - \varepsilon^{1/2} \frac{\sqrt{\alpha_0}}{(2l + 1)} \left(l^2 + 6l + 3 + \frac{(l + 1)^2}{|E_0|} \right) - \frac{lR}{(2l + 1)Q} \right] \frac{b_{lm}}{R}. \end{aligned} \quad (23)$$

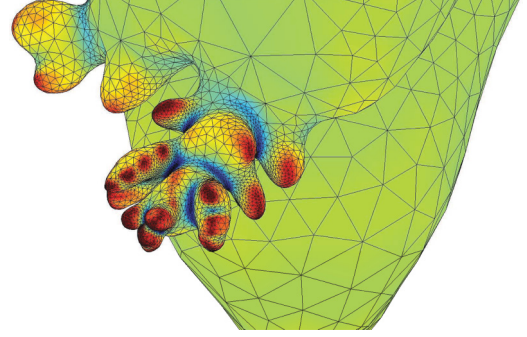


FIG. 2. (Color online) Detail of the shape of the plasma at $t = 0.1769$.

If $Q(t) = Q$, it is easy to check (see the Appendix, Sec. 1) that

$$R(t) \approx \left(\frac{3|Q|}{4\pi} t \right)^{1/3}, \quad (17)$$

for the early stages of the discharge and as long as $R \ll \frac{|Q|}{\varepsilon}$. This is in agreement with predictions based on continuum streamer models [26,27]. If the position of the front as well as the charge density are changed by a small amount, the perturbed quantities can be parametrized as

$$r(\theta, \phi, t) = R(t) + \delta S(\theta, \phi, t), \quad (18)$$

$$\sigma(\theta, \phi, t) = -\frac{Q(t)}{4\pi R^2(\theta, \phi, t)} + \delta \Sigma(\theta, \phi, t), \quad (19)$$

where δ is a small parameter. The angles θ (colatitude) and ϕ (longitude) are the usual spherical coordinate ones. The z axis is in the vertical direction. For convenience we write the surface perturbation in terms of spherical harmonics as

$$S = \sum_{l=1}^{\infty} \sum_{m=-l}^l s_{lm}(t) Y_{lm}(\theta, \phi), \quad (20)$$

and the surface charge density perturbation as

$$\Sigma = -\sum_{l=1}^{\infty} \sum_{m=-l}^l \left(\frac{2l + 1}{R} b_{lm} + \frac{Q(t)}{4\pi R^2} \frac{l + 1}{R} s_{lm} \right) Y_{lm}(\theta, \phi), \quad (21)$$

where the coefficients $s_{lm}(t)$ and b_{lm} have to be determined. Making a standard expansion of the dynamics contour model equations (5) and (6) (see the Appendix, Sec. 2), up to linear terms, we get the equations for the particular mode evolution

$$\begin{aligned} \frac{ds_{lm}}{dt} = & \left[\varepsilon^{1/2} \frac{\sqrt{\alpha_0} \operatorname{sgn}[Q(t)]}{|E_0|} \left(1 + \frac{1}{|E_0|} \right) - 1 \right] \frac{(l + 1)}{R} b_{lm} \\ & + \left[\varepsilon^{1/2} \sqrt{\alpha_0} \left(1 + \frac{1}{|E_0|} \right) - E_0 - \frac{\varepsilon(l + 2)}{R} \right] \frac{(l - 1)}{R} s_{lm}, \end{aligned} \quad (22)$$

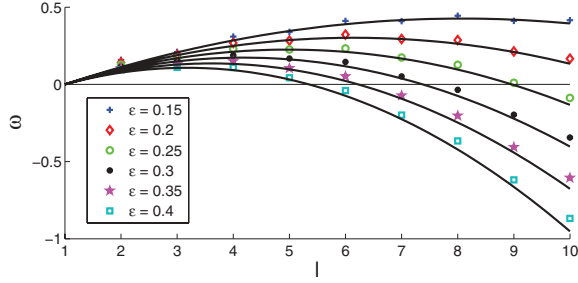


FIG. 3. (Color online) Analytical (in black) and numerical dispersion curves for different values of the diffusion coefficient ε . The abscissa corresponds to the spherical harmonics number, and the ordinate to the growth rate for that mode.

We can get information about the growth of different modes by analyzing two special limits. First we study the limit of ideal conductivity. It corresponds to $\varrho \rightarrow 0$, and hence, from (23), we can conclude that $b_{lm} \rightarrow 0$. This is the case when in the limit of very high conductivity, the electric field inside goes to zero ($E_v^- \rightarrow 0$), as we approach to the behavior of a perfect conductor. If we consider that $Q(t) = Q_0$ is constant or its variation in time is small compared with the evolution of the modes [which also implies $I(t) \rightarrow 0$], and the same for the radius of the front $R(t) = r_0$, we look for a solution $s_{lm} = \exp(\omega t)$, $\varphi_n = 0$, to (22), and get a discrete dispersion relation of the form

$$\omega = \left[\varepsilon^{1/2} \sqrt{\alpha_0} \left(1 + \frac{1}{|E_0|} \right) - E_0 - \frac{\varepsilon(l+2)}{r_0} \right] \frac{(l-1)}{r_0}, \quad (24)$$

with a maximum at

$$l = l_{\max} \simeq \frac{|E_0| r_0}{2\varepsilon}, \quad (25)$$

for $\varepsilon \ll 1$. For a small enough conductivity $\varrho \rightarrow \infty$, we find $b_{lm} = -E_0 s_{lm} (l+1)/(2l+1)$, and with $s_{lm} = \exp(\omega t)$, (22) yields

$$\omega = \left[\varepsilon^{1/2} \sqrt{\alpha_0} \left(1 + \frac{1}{|E_0|} \right) - E_0 \right] \frac{(l^2 - 3l - 2)}{(2l+1)r_0} - \frac{\varepsilon(l+2)(l-1)}{r_0^2}, \quad (26)$$

with a maximum at

$$l = l_{\max} \simeq \frac{|E_0| r_0}{\varepsilon}, \quad (27)$$

for $\varepsilon \ll 1$. Note that the dispersion relation does not depend on m . The finite resistivity cases lay between those limits. In Fig. 3 we have plotted the analytical curves given by (24) for different values of ε and the results of numerical calculations for a perfect conductor. The numerical calculations are done in the following way: We take a spherical front and introduce a small perturbation in the form of a spherical harmonic Y_{lm} times a small parameter δ . By tracing the evolution of that front using the numerical method reported in Sec. II (see the Appendix, Sec. 4, for details about the numerical method) and tracking the maximum distance of the points of the surface to the center of the sphere, we find that it is the radius of the unperturbed sphere plus a perturbation with an amplitude that

grows exponentially $\delta \exp(\omega_l t) Y_{lm}$. Hence, we can compute the dispersion relation ω_l as a function of l . In Fig. 4 in the Appendix we present the initial perturbed sphere with $Y_{10,10}$ and the result of the evolution after some time.

The dispersion curve allows one to predict the expected number of branches that will develop. Each branch will undergo also a further split and so on, propagating to the smaller scales. However, it cannot run forever, as there is a limitation and the model does not take into account the energy radiated, the heat exchange, and the other phenomena that will start to play an important role at later stages of the discharge.

IV. CONCLUSIONS

The results presented in this work confirm the hypothesis that at the earlier stages of an electric discharge, the main driving forces are diffusion and electrical drift, first anticipated in Ref. [8]. The expressions obtained for the growth rate of the modes, given by (24) and (26), enables one to predict the number of forks that one can expect in an electric discharge provided the electric field and the diffusion constant are known by other means. But, the opposite can be worked out: From the numbers of fingers observed, we can, for example, infer the electric field if the charge density at the interface and the diffusion constant are known. This has been done for the 2D case [21]. Here follows a brief account of the 2D experiment discussed there. A discharge is created on a dielectric surface using a positive tip and branching is observed. The electric potential along the streamers is measured using Pockels crystals, laser pulses, and a CCD camera. Using typical values for the mobility μ_e and E_0 , from the dispersion relations the diffusion coefficient D was estimated and thus the number of fingers one may expect in such experiments. This number is calculated from the maxima of the dispersion relations. Counting the number of real fingers in the experimental pictures [22], the number was around 20, and our prediction was $n \approx 14$.

The model presented here, when considered for a perturbation of a planar front, predicts an instability in the form of fingers, whose spacing agrees with the prediction of the full minimal streamer model, which was compared in Ref. [28] with available experimental data by Raether [29]. The separation of the fingers turns out to be $\lambda_{\max} \sim (D_e/E_0)^{0.33}$, at a given gas pressure, where E_0 is the applied electric field. The experimental values for the exponent for nonattaching gases such as N_2 and Ar are 0.32 and 0.34, respectively. This prediction allows one to also compute the local electric field if the number of fingers is known.

For the 3D case, there is a lack of quantitative experimental data for electric field along the discharge. The charge density could be used to calculate the electric field and it might be obtained from Stark's effect measurements, but we have not found any data available. Thus an effective diffusion coefficient might be approximately calculated, and the number of fingers predicted. Or alternatively, from the branching observed, by using formula (25) or (27) the effective diffusion could be obtained if the local electric field is known or vice versa, the local electric field can be inferred if the effective electron diffusion coefficient is given.

In conclusion, the results presented in this work may contribute to achieving one of the main goals, both in the laboratory and in nature, of the current research in the area of electric discharges: bringing the field from a qualitative and descriptive era to a quantitative one.

ACKNOWLEDGMENTS

This work has been supported by the Spanish Ministerio de Ciencia e Innovación under projects AYA2009-14027-C07-04, AYA2011-29336-C05-03, and MTM2011-26016. We also thank the anonymous referee for pointing out some references on the mathematical analysis of moving boundary problems.

APPENDIX

1. Solutions with symmetry

The electric potential created by a negative surface charge distribution with radial symmetry at the distance R is found by solving

$$\Delta V = \sigma \delta(R). \quad (\text{A1})$$

The solution turns out to be in spherical coordinates

$$V(\mathbf{x}) = \begin{cases} C/|\mathbf{x}|, & |\mathbf{x}| > R \\ C/R, & |\mathbf{x}| \leq R, \end{cases} \quad (\text{A2})$$

where C will be determined by the condition of the electric field jump (4) at the surface. From the potential solution we can compute the electric field

$$E_v^- = 0, \quad E_v^+ = \frac{C}{R^2}. \quad (\text{A3})$$

For the current density, the solution of (3) gives

$$\mathbf{j} = \frac{I(t)}{4\pi R^3} \mathbf{R},$$

and finally using (6) and the fact that $v_N = dR/dt$ and $\kappa = 2/R$, we get

$$\frac{\partial \sigma}{\partial t} + \frac{2}{R} \frac{\partial R}{\partial t} \sigma = -\frac{I(t)}{4\pi R^2}. \quad (\text{A4})$$

This equation can be easily solved. We can write it as

$$\frac{\partial(R^2 \sigma)}{\partial t} = -\frac{I(t)}{4\pi},$$

to get

$$\sigma = -\frac{Q(t)}{4\pi R^2}, \quad \text{with} \quad Q(t) = \int_0^t I(t') dt',$$

where we have assumed that $\sigma(0) = 0$. Now we can see from the condition (4) that $C = Q(t)/4\pi$, so

$$E_v^+ = \frac{Q(t)}{4\pi r^2}.$$

Then the interface evolves according to (5) as

$$\frac{dR}{dt} = -\left(\frac{Q(t)}{4\pi R} + 2\varepsilon\right) \frac{1}{R} + 2\varepsilon^{1/2} \sqrt{\alpha(|E_v^+|)}. \quad (\text{A5})$$

It can be seen that diffusion will accelerate the front through the term $\varepsilon^{1/2}$ as far as the curvature becoming small. A

perturbation of the front will be made smooth by this term, meanwhile electric field will do the opposite.

Next, we shall analyze two limiting cases. First the case where

$$R^2 \ll \frac{|Q(t)|}{8\pi \varepsilon^{1/2} \sqrt{\alpha[|Q(t)/4\pi R^2]}} \quad \text{and} \quad \varepsilon \ll \frac{|Q(t)|}{8\pi R}. \quad (\text{A6})$$

Then expression (A5) results in

$$\frac{dR}{dt} \approx -\frac{Q(t)}{4\pi R^2}, \quad (\text{A7})$$

so

$$R(t) \approx \left(R(0)^3 - \int_0^t 3Q(t')/4\pi dt'\right)^{1/3}. \quad (\text{A8})$$

For the particular case $Q(t) = Q$ is constant,

$$R(t) \approx [R(0)^3 - 3tQ/4\pi]^{1/3}. \quad (\text{A9})$$

The second case is the opposite. If

$$R \gg \frac{|Q(t)|}{8\pi \varepsilon^{1/2} \sqrt{\alpha[|Q(t)/4\pi R^2]}} \quad \text{and} \quad \varepsilon \ll \frac{|Q(t)|}{8\pi R}, \quad (\text{A10})$$

we now have

$$\frac{dR}{dt} \approx 2\varepsilon^{1/2} \sqrt{\alpha[|Q(t)/4\pi R^2]}. \quad (\text{A11})$$

For the particular case $Q(t) = Q$, we obtain

$$R(t) = \left[\frac{|Q|}{2\pi} \log\left(4t \sqrt{\frac{\pi\varepsilon}{|Q|}}\right)\right]^{1/2}. \quad (\text{A12})$$

2. Stability analysis

If the spherical symmetry is perturbed by a small amount, some instabilities will start growing as shown in the figures. We will study in this section which instability modes are going to prevail during the front evolution.

If the position of the front as well as the charge density are changed by a small amount, the perturbed quantities can be parametrized as

$$r(\theta, \phi, t) = R(t) + \delta S(\theta, \phi, t), \quad (\text{A13})$$

$$\sigma(\theta, \phi, t) = -\frac{Q(t)}{4\pi R^2(\theta, \phi, t)} + \delta \Sigma(\theta, \phi, t), \quad (\text{A14})$$

where $R(t)$ is given by Eq. (A5), i.e., the radial symmetrical front, and δ is our bookkeeping small parameter for the expansions which follow. The angles θ and ϕ are the spherical coordinate ones.

We will start calculating the correction to the electric field due to the geometrical perturbation of the surface and the extra charge deposited on it. The electric potential will be up to δ order

$$\Phi(\mathbf{x}) = V(\mathbf{x}) + \delta V_p(\mathbf{x}),$$

with V being the solution we used in the previous section for the symmetrical problem. The term $V_p(\mathbf{x})$ will satisfy the equation

$$\Delta V_p = O(\delta),$$

and further on, we will change coordinates to

$$\mathbf{x} \longrightarrow \tilde{\mathbf{x}} = \mathbf{x} \frac{R(t)}{r(\theta, \phi, t)},$$

so the perturbed surface becomes a sphere of radius $R(t)$. Now at zero order V_p satisfies the Laplace equation with the boundary being a sphere. Hence we have in the new spherical coordinates

$$V_p(\tilde{r}, \theta) = \begin{cases} \sum_{l=1}^{\infty} \sum_{m=-l}^l a_{lm} Y_{lm}(\theta, \phi) \left(\frac{R}{\tilde{r}}\right)^{l+1}, & \tilde{r} > R \\ \sum_{l=1}^{\infty} \sum_{m=-l}^l b_{lm} Y_{lm}(\theta, \phi) \left(\frac{\tilde{r}}{R}\right)^l, & \tilde{r} \leq R, \end{cases} \quad (\text{A15})$$

where it is imposed that V_p remains finite at the origin and at very large distances becomes zero. Note the sums start at $l = 1$, as for $l = 0$ we have just a constant.

Since the potential at the surface position coming from the exterior is

$$\begin{aligned} \Phi(\mathbf{x}_s^+) &= V(\mathbf{x}_s^+) + \delta V_p(\mathbf{x}_s^+) = \frac{Q(t)}{4\pi} \frac{1}{R + \delta S} + \delta V_p(\mathbf{x}_s^+) \\ &= \frac{Q(t)}{4\pi} \left(\frac{1}{R} - \delta \frac{S}{R^2} \right) + \delta V_p(\mathbf{x}_s^+) + O(\delta^2), \end{aligned}$$

and from the interior is

$$\Phi(\mathbf{x}_s^-) = V(\mathbf{x}_s^-) + \delta V_p(\mathbf{x}_s^-) = C(R(t), t) + \delta V_p(\mathbf{x}_s^-),$$

where $C(R(t), t)$ is a function independent of θ , imposing the condition of continuity for the potential, we have

$$V_p(\mathbf{x}_s^+) = V_p(\mathbf{x}_s^-) + S \frac{Q(t)}{4\pi R(t)^2}.$$

If we write the surface perturbation as

$$S = \sum_{l=1}^{\infty} \sum_{m=-l}^l s_{lm}(t) Y_{lm}(\theta, \phi), \quad (\text{A16})$$

we find that the coefficients of the potential in Eq. (A15) are related by

$$a_{lm} = b_{lm} + \frac{Q(t)}{4\pi R^2} s_{lm}, \quad (\text{A17})$$

where $R = R(t)$.

Using expressions (A15)–(A17) and changing back coordinates from $\tilde{\mathbf{x}}$ to \mathbf{x} , the normal components of the electric field at both sides of the surface are

$$\begin{aligned} E_v^+ &= \frac{Q(t)}{4\pi(R + \delta S)^2} + \delta \sum_{l=1}^{\infty} \sum_{m=-l}^l \left(b_{lm} + \frac{Q(t)}{4\pi R^2} s_{lm} \right) \\ &\quad \times \frac{(l+1)}{R} Y_{lm}(\theta, \phi) + O(\delta^2), \end{aligned} \quad (\text{A18})$$

$$E_v^- = -\delta \sum_{l=1}^{\infty} \sum_{m=-l}^l b_{lm} \frac{l}{R} Y_{lm}(\theta, \phi). \quad (\text{A19})$$

Then, from the jump condition (4), the charge perturbation in Eq. (A14) results as

$$\Sigma = - \sum_{l=1}^{\infty} \sum_{m=-l}^l \left(\frac{2l+1}{R} b_{lm} + \frac{Q(t)}{4\pi R^2} \frac{l+1}{R} s_{lm} \right) Y_{lm}(\theta, \phi). \quad (\text{A20})$$

We still need the expression of twice the main curvature at order to find the dynamics of the front. In spherical coordinates, it yields (see, for instance, [30])

$$\kappa = \frac{2}{R} - \frac{2S + \Delta_\omega S}{R^2} \delta + O(\delta^2),$$

where Δ_ω is the Laplace operator on the unit sphere

$$\Delta_\omega = \frac{1}{\sin \theta} \frac{\partial}{\partial \theta} \left(\sin \theta \frac{\partial}{\partial \theta} \right) + \frac{1}{\sin^2 \theta} \frac{\partial^2}{\partial \phi^2}, \quad (\text{A21})$$

which has the property

$$\Delta_\omega Y_{lm} = -l(l+1) Y_{lm}.$$

Also we need the normal component of the velocity up to first order

$$v_N = \mathbf{v} \cdot \mathbf{n} = \frac{dR(t)}{dt} + \delta \frac{\partial S(\theta, t)}{\partial t} + O(\delta^2). \quad (\text{A22})$$

So the contour model equation (5), to first order gives

$$\begin{aligned} \frac{dR}{dt} + \delta \frac{\partial S(\theta, t)}{\partial t} &= - \frac{Q(t)}{4\pi R^2} + \delta S \frac{Q(t)}{2\pi R^3} \\ &\quad - \delta \sum_{l=1}^{\infty} \sum_{m=-l}^l \left(b_{lm} + \frac{Q(t)}{4\pi R^2} s_{lm} \right) \frac{l+1}{R} Y_{lm}(\theta, \phi) \\ &\quad + 2\varepsilon^{1/2} \sqrt{\alpha_0 + \delta \alpha_1} - \varepsilon \left(\frac{2}{R} - \delta \frac{2S + \Delta_\omega S}{R^2} \right), \end{aligned} \quad (\text{A23})$$

where we have written the Townsend function (7) up to first order as $\alpha = \alpha_0 + \delta \alpha_1 + O(\delta^2)$. We can expand that function as

$$\begin{aligned} |E_0 + \delta E_1| e^{-(1/|E_0 + E_1 \delta|)} &\approx |E_0| e^{-(1/|E_0|)} + \delta \operatorname{sgn}(E_0) E_1 \left(1 + \frac{1}{|E_0|} \right) e^{-(1/|E_0|)} \\ &= \alpha_0 + \delta \alpha_1, \end{aligned}$$

so that

$$\begin{aligned} \sqrt{\alpha} &= \sqrt{\alpha_0} + \delta \frac{\alpha_1}{2\sqrt{\alpha_0}} \\ &= \sqrt{\alpha_0} \left[1 + \delta \operatorname{sgn}[Q(t)] \frac{E_1}{2|E_0|} \left(1 + \frac{1}{|E_0|} \right) \right], \end{aligned}$$

being

$$\begin{aligned} E_0 &= \frac{Q(t)}{4\pi R^2}, \\ E_1 &= \sum_{l=1}^{\infty} \sum_{m=-l}^l [b_{lm}(l+1) + E_0 s_{lm}(l-1)] \frac{Y_{lm}(\theta, \phi)}{R}, \end{aligned}$$

obtained from expanding (A18) in δ as $E_v^+ = E_0 + \delta E_1 + O(\delta^2)$.

Taking into account (A5) for the zero order term, we get from (A23),

$$\begin{aligned} \frac{\partial S}{\partial t} &= S \frac{Q(t)}{2\pi R^3} - \sum_{l=1}^{\infty} \sum_{m=-l}^l \left(b_{lm} + \frac{Q(t)}{4\pi R^2} s_{lm} \right) \frac{l+1}{R} Y_{lm} \\ &\quad + \varepsilon \frac{2S + \Delta_\omega S}{R^2} + \varepsilon^{1/2} \frac{\alpha_1}{\sqrt{\alpha_0}}, \end{aligned} \quad (\text{A24})$$

and finally making use of the expansion (A16) for the perturbation S yields (22).

The correction to the charge density evolution comes from (6),

$$\frac{\partial \sigma}{\partial t} + \kappa v_N \sigma = -\frac{1}{\varrho} E_v^- - \frac{I(t)}{4\pi R^2}.$$

We multiply it by $r^2(\theta, \phi, t)$, and substituting the curvature expansion we can write

$$\begin{aligned} \frac{\partial(r^2(\theta, \phi, t)\sigma(\theta, \phi, t))}{\partial t} - r^2(\theta, \phi, t)\frac{\Delta_\omega S}{R^2}v_N\sigma(\theta, \phi, t)\delta \\ = -\frac{r^2(\theta, \phi, t)}{\varrho}E_v^- - \frac{I(t)}{4\pi}. \end{aligned}$$

Note we have used that

$$\begin{aligned} r^2(\theta, \phi, t)v_N\sigma(\theta, \phi, t) &= \frac{r^2(\theta, \phi, t)v_N\sigma(\theta, \phi, t)}{R} \\ &\quad - \frac{Sr^2(\theta, \phi, t)v_N\sigma(\theta, \phi, t)\delta}{R} + O(\delta^2), \end{aligned}$$

following to δ order

$$\frac{\partial(R^2\Sigma)}{\partial t} + \frac{\Delta_\omega S}{R^2}\frac{Q(t)}{4\pi}\frac{dR}{dt} = \frac{R}{\varrho}\sum_{l=1}^{\infty}\sum_{m=-l}^l b_{lm}Y_{lm}(\theta, \phi)l. \quad (\text{A25})$$

Finally, making use of (A5), (A16), and (A20), we get

$$\begin{aligned} -\frac{d}{dt}\left(R(2l+1)b_{lm} + \frac{Q(t)}{4\pi R}(l+1)s_{lm}\right) \\ = \frac{Q(t)}{4\pi R^2}\frac{dR}{dt}l(l+1)s_{lm} + \frac{Rl}{\varrho}b_{lm}, \end{aligned}$$

or after simplifying,

$$\begin{aligned} (2l+1)\frac{db_{lm}}{dt} + \frac{Q(t)}{4\pi R^2}(l+1)\frac{ds_{lm}}{dt} \\ = -(l+1)(l-1)\frac{Q(t)}{4\pi R^3}\frac{dR}{dt}s_{lm} - (l+1)\frac{I(t)}{4\pi R^2}s_{lm} \\ - \frac{(2l+1)}{R}\frac{dR}{dt}b_{lm} - \frac{l}{\varrho}b_{lm}. \end{aligned}$$

Using (A5), (A24), and (22),

$$\begin{aligned} (2l+1)\frac{db_{lm}}{dt} + (l+1)E_0\left\{\left[\varepsilon^{1/2}\frac{\sqrt{\alpha_0}\text{sgn}[Q(t)]}{|E_0|}\left(1 + \frac{1}{|E_0|}\right) - 1\right]\frac{(l+1)}{R}b_{lm}\right. \\ \left. + \left[\varepsilon^{1/2}\sqrt{\alpha_0}\left(1 + \frac{1}{|E_0|}\right) - E_0 - \frac{\varepsilon(l+2)}{R}\right]\frac{(l-1)}{R}s_{lm}\right\} \\ = (l+1)(l-1)\frac{E_0}{R}\left[E_0 + \frac{2\varepsilon}{R} - 2\varepsilon^{1/2}\sqrt{\alpha_0}\right]s_{lm} - (l+1)\frac{I(t)}{4\pi R^2}s_{lm} + \frac{(2l+1)}{R}\left[E_0 + \frac{2\varepsilon}{R} - 2\varepsilon^{1/2}\sqrt{\alpha_0}\right]b_{lm} - \frac{l}{\varrho}b_{lm}, \end{aligned}$$

and after rearranging the terms Eq. (23) follows. Thus the time evolution of each particular mode has been obtained and it is governed by (22) and (23).

3. Special limits

We can get information of the dispersion curve by analyzing two special limits. First we study the limit of ideal conductivity. It corresponds to $\varrho \rightarrow 0$, and hence, from (23), we can conclude that $b_{lm} \rightarrow 0$. This is the case when in the limit of very high conductivity, the electric field inside goes to zero ($E_v^- \rightarrow 0$), as we approach the behavior of a perfect conductor. If we consider that $Q(t) = Q_0$ is constant or its variation in time is small compared with the evolution of the modes [which also implies $I(t) \rightarrow 0$], and the same for the radius of the front $R(t) = r_0$, we look for a solution $s_{lm} = \exp(\omega t)$, $\varphi_n = 0$, to (22), and get the discrete dispersion relation (24).

Next we consider the limit of finite resistivity, but such that the total charge is constant at the surface, or varies very slowly. Writing (23) as

$$\begin{aligned} (2l+1)\frac{d}{dt}(rb_{lm}) &= -\frac{d}{dt}\left(\frac{Q(t)}{4\pi r}(l+1)s_{lm}\right) \\ &\quad - \frac{Q(t)}{4\pi r^2}\frac{dr}{dt}l(l+1)s_{lm} - \frac{rl}{\varrho}b_{lm}, \end{aligned}$$

we now have

$$\frac{db_{lm}}{dt} = -\frac{Q_0}{4\pi r_0^2}\frac{(l+1)}{(2l+1)}\frac{ds_{lm}}{dt} - \frac{l}{(2l+1)\varrho}b_{lm}. \quad (\text{A26})$$

For a small enough conductivity $\varrho \rightarrow \infty$ so no extra charge reaches the surface, we find $b_{lm} = -E_0s_{lm}(l+1)/(2l+1)$, and with $s_{lm} = \exp(\omega t)$, Eq. (22) yields the relation (26).

4. Brief explanation of the numerical method

Our interest in the evolution of the surface suggests the use of the boundary element method to calculate the velocity at the interface. At any given time $t > 0$, we approximate the free boundary $\partial\mathcal{D}(t)$ with a triangular mesh. On each node of the mesh we approximate the various physical quantities that are defined on the surface (charge density, curvature, velocity) with elementwise constant functions over a ‘‘virtual’’ element centered in each node with an area equal to one-third of the total area of the elements that share the node (see [31]). We also use the nodes of the mesh as collocation points.

The general description of how we solve the equations is as follows: First we calculate the curvature κ in each node of the mesh; second, we calculate the surface charge density (and hence the electric field at the boundary) by solving, using the boundary element method, the integral equations relating the surface charge density and the electric field Eqs. (13)

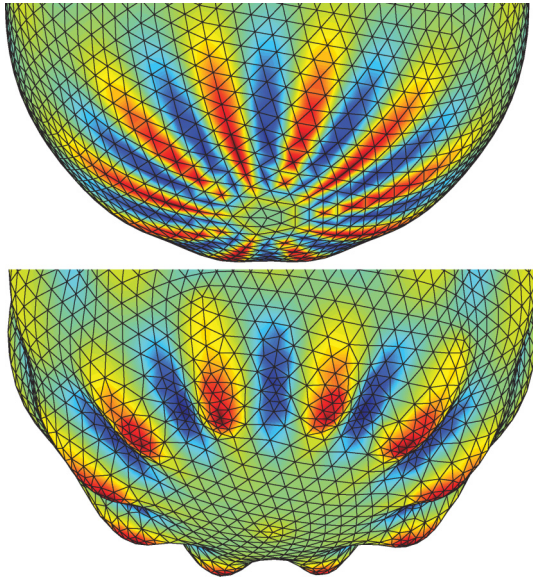


FIG. 4. (Color online) Evolution of a perturbed sphere of plasma for integrated surface charge $Q = 25$ and diffusion coefficient $\varepsilon = 0.02$. Top: the sphere is initially perturbed with the spherical harmonic $Y_{10,10}$ and $\delta = 0.01$. Bottom: shape of the plasma at $t = 0.1279$.

and (14). Given the resulting velocity \mathbf{v} , we move the points of the surface using the explicit Euler scheme and regularize

and refine the mesh if necessary. In order to be able to resolve tips and tip splitting with the necessary precision, an adaptive technique is involved. The adaptivity is achieved in two ways: (1) by moving the nodes towards regions of large curvature and (2) by splitting triangles into three subtriangles. The first procedure consists in adding a tangential “spring force” between neighbor nodes, which depends on the local curvature. In this way, once a tip starts to appear, it tends to attract its neighbors and the process induces a clustering of nodes in the critical regions. The second procedure is done in such a way that the quality of the triangulation is not lost and the triangles do not become too deformed. Further details on these procedures can be found in Refs. [23,24]. Finally, we remark that boundary conditions, such as electric field far away from the streamer, do not need to be imposed separately since they automatically appear in the boundary integral formulation of the problem.

Furthermore, in order to verify the correctness of our dispersion relation, we take spheres and introduce a small perturbation in the form of a spherical harmonic Y_{lm} times a small parameter δ . By tracing the evolution of the maximum distance of the points of the surface to the center of the sphere, we find that it is the radius of the unperturbed sphere plus a perturbation with an amplitude that grows exponentially, $\delta \exp(\omega_l t) Y_{lm}$. Hence, we can compute the dispersion relation ω_l as a function of l . In Fig. 4 we present the initial perturbed sphere with $Y_{10,10}$ and the result of the evolution after some time.

-
- [1] Y. P. Raizer, *Gas Discharge Physics* (Springer, Berlin 1991).
- [2] H. Raether, *Electron Avalanches and Breakdown in Gases* (Butterworths, London, 1964).
- [3] V. P. Pasko, *Nature (London)* **423**, 927 (2003).
- [4] S. K. Dhali and P. F. Williams, *Phys. Rev. A* **31**, 1219 (1985); *J. Appl. Phys.* **62**, 4696 (1987).
- [5] P. A. Vitello, B. M. Penetrante, and J. N. Bardsley, *Phys. Rev. E* **49**, 5574 (1994).
- [6] A. N. Lagarkov and I. M. Rutkevich, *Ionization Waves in Electric Breakdown on Gases* (Springer-Verlag, New York, 1994).
- [7] U. Ebert, W. van Saarloos, and C. Caroli, *Phys. Rev. Lett.* **77**, 4178 (1996); *Phys. Rev. E* **55**, 1530 (1997).
- [8] M. Arrayás, U. Ebert, and W. Hundsdorfer, *Phys. Rev. Lett.* **88**, 174502 (2002).
- [9] C. Montijn, U. Ebert, and W. Hundsdorfer, *Phys. Rev. E* **73**, 065401 (2006).
- [10] N. Liu and V. P. Pasko, *J. Geophys. Res.* **109**, A04301 (2004).
- [11] M. Arrayás, M. A. Fontelos, and J. L. Trueba, *Phys. Rev. Lett.* **95**, 165001 (2005).
- [12] U. Ebert *et al.*, *Nonlinearity* **24**, C1 (2011).
- [13] A review of the state of 3D streamer simulations has been recently published in a special issue on Computational Plasma Physics in *J. Comput. Phys.* **231**, 717 (2012). In particular, the article by V. I. Kolobov and R. R. Arslanbekov, *ibid.* **231**, 839 (2012) and the one by A. Luque and U. Ebert, *ibid.* **231**, 904 (2012).
- [14] S. Tanveer, L. Schafer, F. Brau, and U. Ebert, *Physica D* **238**, 888 (2009).
- [15] S. Tanveer, C.-Y. Kao, L. Schafer, F. Brau, and U. Ebert, *Physica D* **239**, 1542 (2010).
- [16] M. Arrayás, M. A. Fontelos, and J. L. Trueba, *J. Phys. D* **39**, 5176 (2006).
- [17] M. Arrayás, J. P. Baltanás, and J. L. Trueba, *J. Phys. D* **41**, 105204 (2008).
- [18] A. Luque and U. Ebert, *Phys. Rev. E* **84**, 046411 (2011).
- [19] C. Li, J. Teunissen, M. Nool, W. Hundsdorfer, and U. Ebert, *Plasma Sources Sci. Technol.* **21**, 055019 (2012).
- [20] M. Arrayás, M. A. Fontelos, and C. Jiménez, *Phys. Rev. E* **81**, 035401(R) (2010).
- [21] M. Arrayás and M. A. Fontelos, *Phys. Rev. E* **84**, 026404 (2011).
- [22] D. Tanaka *et al.*, *J. Phys. D: Appl. Phys.* **42**, 075204 (2009).
- [23] M. A. Fontelos, V. J. García-Garrido, and U. Kindelán, *SIAM J. Appl. Math.* **71**, 1941 (2011).
- [24] M. A. Fontelos, U. Kindelán, and O. Vantzou, *Phys. Fluids* **20**, 092110 (2008).
- [25] See Supplemental Material at <http://link.aps.org/supplemental/10.1103/PhysRevE.86.066407> for the development of multiple branching.
- [26] M. Arrayás, M. A. Fontelos, and J. L. Trueba, *Phys. Rev. E* **71**, 037401 (2005).
- [27] A. S. Kyuregyan, *Phys. Rev. Lett.* **101**, 174505 (2008).
- [28] M. Arrayás, M. A. Fontelos, and J. L. Trueba, *Phys. Rev. Lett.* **101**, 139502 (2008).
- [29] H. Raether, *Z. Phys.* **112**, 464 (1939).
- [30] M. Fontelos and A. Friedman, *Arch. Ration. Mech. Anal.* **172**, 267 (2004).
- [31] A. Z. Zinchenko, M. A. Rother, and R. H. Davis, *Phys. Fluids* **9**, 1493 (1997).